

## ⓘ The Megacity Lagos and Three Decades of Urban Heat Island Growth ⓘ

R. BASSETT,<sup>a</sup> P. J. YOUNG,<sup>a,c</sup> G. S. BLAIR,<sup>b,c</sup> F. SAMREEN,<sup>b</sup> AND W. SIMM<sup>b</sup>

<sup>a</sup> Lancaster Environment Centre, Lancaster University, Lancaster, United Kingdom

<sup>b</sup> School of Computing and Communications, Lancaster University, Lancaster, United Kingdom

<sup>c</sup> Centre of Excellence for Environmental Data Science, Lancaster University, Lancaster, United Kingdom

(Manuscript received 12 March 2020, in final form 22 September 2020)

**ABSTRACT:** Lagos, Nigeria, is rapidly urbanizing and is one of the fastest-growing cities in the world, with a population that is increasing at almost 500 000 people per year. Yet the impacts on Lagos's local climate via its urban heat island (UHI) have not been well explored. Considering that the tropics already have year-round high temperatures and humidity, small changes are very likely to tip these regions over heat-health thresholds. Using a well-established model, but with an extended investigation of uncertainty, we explore the impact of Lagos's recent urbanization on its UHI. Following a multiphysics evaluation, our simulations, against the background of an unusually warm period in February 2016 (during which temperatures regularly exceeded 36°C), show a 0.44°C ensemble-time-mean increase in nighttime UHI intensity between 1984 and 2016. The true scale of the impact is seen spatially as the area over which ensemble-time-mean UHIs exceed 1°C was found to increase steeply from 254 km<sup>2</sup> in 1984 to 1572 km<sup>2</sup> in 2016. The rate of warming within Lagos will undoubtedly have a high impact because of the size of the population (12+ million) already at risk from excess heat. Significant warming and modifications to atmospheric boundary layer heights are also found in rural areas downwind, directly caused by the city. However, there is limited long-term climate monitoring in Lagos or many similarly expanding cities, particularly in the tropics. As such, our modeling can only be an indication of this impact of urbanization, and we highlight the urgent need to deploy instrumentation.

**KEYWORDS:** Heat islands; Regional models; Anthropogenic effects; Land use; Urban meteorology

### 1. Introduction

At the current global rate, 2.5 billion more people will live in urban areas by 2050 (United Nations 2015). Ninety percent of this increase is expected to occur in Africa and Asia, whose tropical populations' exposure to excess heat is significantly underestimated; with year-round high temperatures and humidity, small changes to climate in the tropics are likely to tip these regions over heat-health thresholds (Mora et al. 2017). Lagos, Nigeria, the focus of this paper, is one of many examples in the tropics where the rate of urbanization far exceeds global averages. Located in West Africa on the Gulf of Guinea and within a tropical savanna climate (pronounced wet and dry seasons), its growth is being driven by its port, oil exploration, large-scale infrastructure developments and high rural–urban migration rates (Opoko and Oluwatayo 2014). Already Lagos's population has risen from 1.4 million in 1970 to 12.6 million in 2014 with a current growth rate of 3.5% (United Nations 2015). Some end-of-century projections put Lagos's population close to 100 million (Hoornweg and Pope 2017).

Yet, insufficient observations in Nigeria means understanding environmental risks is challenging (Alens 2014).

Inadvertent effects of large, rapid urbanization are well documented globally and include loss of vegetation and ecosystems (Grimm et al. 2008; Seto et al. 2012; Ajibola et al. 2012; Obiefuna et al. 2013), degradation of water (Ouyang et al. 2006; McGrane 2016) and air quality (Han et al. 2016), flooding (Adeloye and Rustum 2011), and modification of the local climate (Kalnay and Cai 2003). Socially, impacts include housing shortages, poverty, and poor living conditions (Opoko and Oluwatayo 2014; Jiboye and Ogunshakin 2011). While one of the primary impacts of urbanization, the urban heat island (UHI) effect, has been extensively documented in tropical areas of Asia and South America (Roth 2007; Santamouris 2015), little research has been conducted in Lagos or many similarly expanding cities in Africa.

UHIs are caused by human-driven changes to the physical processes responsible for exchange of energy and momentum between the surface and atmosphere. UHI intensities (UHII) for air temperatures are largest at night under clear, calm conditions (Oke 1982; Morris et al. 2001) and are a function of city form and size (Oke 1973). UHIs have been shown to increase air temperatures in tropical environments by an average maximum of 3°C, and on occasions in excess of 8°C (Santamouris 2015). In tropical regions, UHII are generally lower than comparably sized temperate cities and experience

ⓘ Denotes content that is immediately available upon publication as open access.

ⓘ Supplemental information related to this paper is available at the Journals Online website: <https://doi.org/10.1175/JAMC-D-20-0059.s1>.

Corresponding author: Richard Bassett, r.bassett@lancaster.ac.uk

DOI: 10.1175/JAMC-D-20-0059.1



UHII variation between seasons, with larger urban–rural temperature differences usually found in the dry seasons (Roth 2007; Santamouris 2015). The UHII of a city may increase over time due to urbanization (Grossman-Clarke et al. 2010), climate change, or a combination (Wilby 2008; McCarthy et al. 2010; Zhao et al. 2014). The UHI is also dynamic and warmth from a city can be advected several kilometers downwind (Bassett et al. 2016).

While UHIs may benefit societies in cool climates (e.g., reducing heating demands (Azevedo et al. 2016), in hot climates the UHI may cause exceedances of heat-health risk thresholds and even mortality (Mora et al. 2017; Heaviside et al. 2017). These impacts become particularly prevalent when heat waves and the UHI effect are combined (Li and Bou-Zeid 2013). For instance, one estimate suggested that the UHI was responsible for half the excess mortality in some regions during the 2003 European heat wave (Heaviside et al. 2016).

Despite an awareness of these health risks, and often being most at risk from environmental change impacts, a lack of observations and technology barriers in developing countries mean there are comparably fewer UHI studies, particularly in Africa. For example, a Web of Knowledge (<https://wok.mimas.ac.uk/>) search (on 30 October 2019) for the terms “urban heat island,” yields 6691 results, whereas refining for “Nigeria” reduces this to only 19. Of studies specific to Lagos, the majority use remote sensing techniques to quantify surface, not air temperatures (e.g., Simwanda et al. 2019; Dissanayake et al. 2019; Ayanlade and Jegede 2015). We found only a single UHI monitoring study that had deployed air temperature observations (Ojeh et al. 2016). While this study reported a large UHI of up to 7°C in Lagos, it was unable to show spatial variability, and the temporal length of the monitoring was too short to show any UHII growth due to urbanization.

Given its vulnerability to small changes in climate and projected rate of urbanization, there is therefore an urgent need to understand Lagos’s UHI growth. We choose to use the regional climate Weather Research and Forecasting (WRF) Model (Skamarock et al. 2008) to simulate the urbanization effect on local climate in Lagos due to its ability to reproduce spatial and temporal UHI patterns that have been extensively evaluated globally (e.g., Miao et al. 2009; Grossman-Clarke et al. 2010; Chen et al. 2014), and more specifically in tropical environments (e.g., Morris et al. 2017; Doan and Kusaka 2018; Li et al. 2013). Through modeling we hope not only highlight the scale of Lagos’s UHI growth but also draw urgent attention to the lack of long-term UHI observations in Lagos and similarly expanding cities.

## 2. Methods

### a. Mapping Lagos’s urbanization

Three clear-sky Landsat satellite images were taken from *Landsat 5* (18 December 1984), *Landsat 7* (6 February 2000), and *Landsat 8* (26 December 2016) (data available from <https://earthexplorer.usgs.gov/>), chosen based on available Landsat images, that is, limited by cloud cover. The following steps

were taken to process the satellite images for use in the WRF Model. (i) Visual analysis was conducted on the red band of each image (and compared with visible satellite images from Google Maps) to identify the approximate wavelength ranges corresponding to urban and rural areas. The R package “segmented” (<https://cran.r-project.org/web/packages/segmented/segmented.pdf>) was then used to determine the breakpoint between these groupings for each image. An example of this approach is provided in Fig. 1a. (ii) The normalized difference vegetation index (NDVI) was calculated within the urban areas for each image,

$$\text{NDVI} = \frac{(\text{NIR} - \text{red})}{(\text{NIR} + \text{red})},$$

where NIR and “red” are the respective spectral reflectances in the near-infrared and red visible wavelengths. Because vegetation strongly absorbs visible wavelengths but reflects near-infrared wavelengths, NDVI effectively provides a dimensionless value of “greenness.” The inverse of this can therefore be used as a proxy for urban intensity. (iii) Visual checks were conducted to remove erroneous urban classifications; for example, sand exhibited similar spectral characteristics to urban. (iv) The resulting NDVI values for each image were normalized, and checks were made between each period, that is, an area categorized as vegetation in 2016 would unlikely be urban in 1984. (v) Comparisons were made between our 2016 NDVI image and a 2014 Global Human Settlement (GHS; <https://ghsl.jrc.ec.europa.eu/index.php>) classification, shown in Fig. 1b. Both methods produce very similar urban extents. However, we argue that our method is improved over the GHS because we have more differentiation within the urban areas, whereas the GHS is skewed toward 0% or 100% urban, and GHS is known to contain erroneous classifications in arid environments (Pesaresi et al. 2016). In our study area, GHS classifies some beaches as urban (cf. the bottom of each domain in Fig. 1b). We appreciate that GHS is a global classification and small-scale corrections may not be feasible. (vi) Nonurban areas were populated with vegetation categories from the default WRF land use (Moderate Resolution Imaging Spectroradiometer). Although the method is subjective, urban NDVI values were split into three WRF urban land-use categories (low-density residential, high-density residential, and industrial and commercial) on the basis of equal size groupings for 2016, and these same threshold values (0–0.46, 0.46–0.57, and 0.57–1) were used for 1984 and 2000. (vii) After creating three urbanization cases, simply referred to as 1984, 2000, and 2016, a final nonurban case (NOURB) was generated. Here all urban land use was replaced with the WRF vegetation category “cropland/natural vegetation mosaic.”

The resulting urban land-use cases are presented in Fig. 2. We recognize some limitations in our land-use classifications: (i) the land-use was based on images from different satellites (*Landsat 5*, *Landsat 7*, and *Landsat 8*), meaning subtle differences in wavelength bands may alter the classifications; (ii) for the NOURB case the urban land use was replaced with a single vegetation category, meaning rural homogeneity may incorrectly be presumed; and (iii) we apportion regions into three

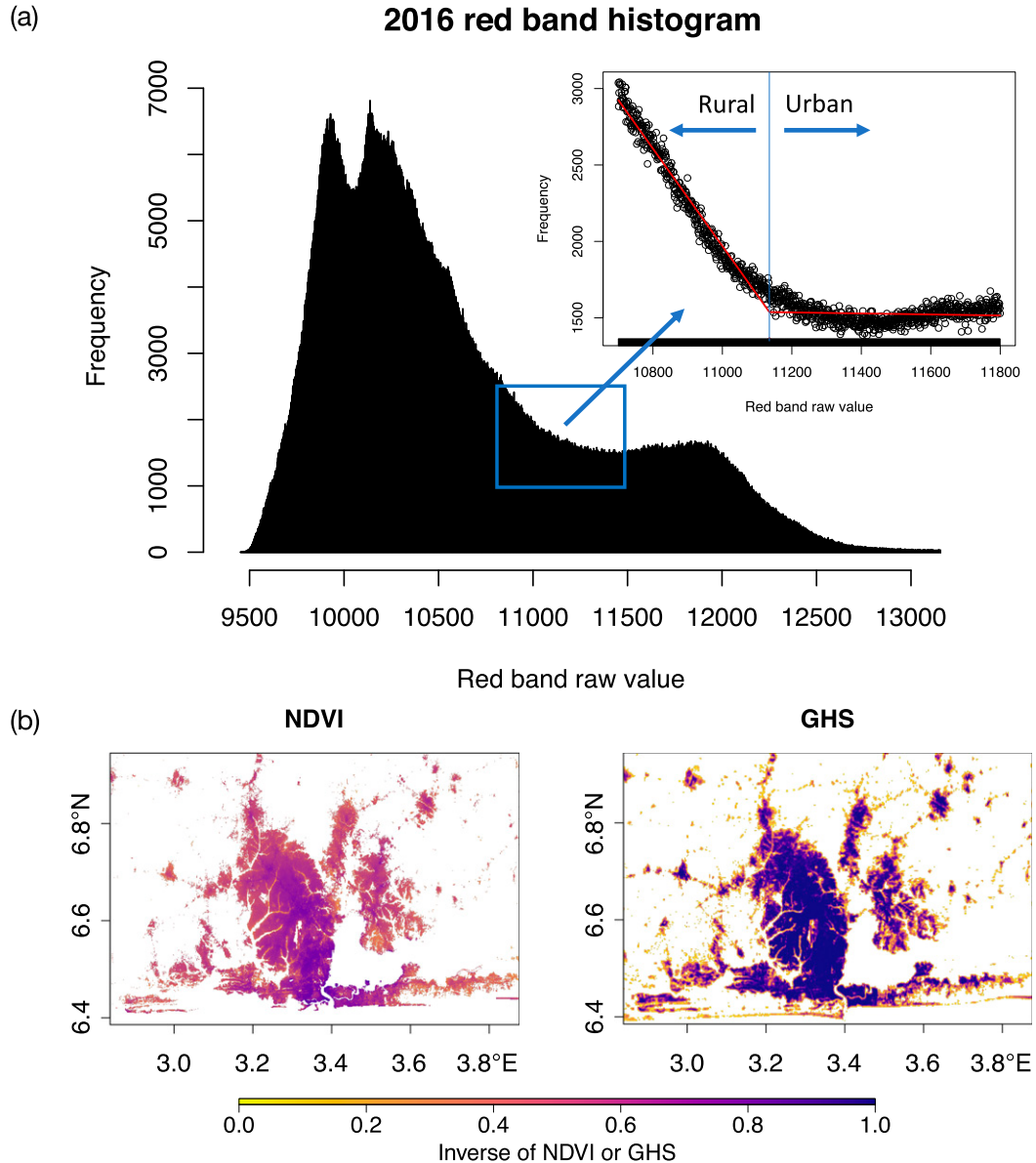


FIG. 1. (a) Example use of breakpoint analysis to determine the red-band values corresponding to rural or urban for the 2016 case. (b) Comparison between the 2016 NDVI image and a 2014 GHS classification.

urban categories when in reality more urban configurations will exist.

#### *b. WRF configuration and evaluation*

WRF, version 3.9.1.1 ([Skamarock et al. 2008](#)), was configured using four two-way nested domains with increasing resolution ([Fig. 3a](#)). The domains had west–east and south–north sizes of 112, 112, 112, and 151 grid cells at 27-, 9-, 3-, and 1-km resolution, respectively. The outer model domain covered a large region of West Africa, allowing WRF to internally generate realistic weather conditions. The use of nests enables increased model resolution over the study area without significantly increasing computational time.

February 2016 was chosen for our analyses because it represented a dry and unusually warm period for Lagos. The city lies within the Köppen classification tropical savanna, with pronounced wet (April–October) and dry (November–March) seasons. Average maximum temperatures range between 29° (wet season) and 34°C (dry season), with annual mean precipitation of 1700 mm ([Ojeh et al. 2016](#)). From reviews of tropical UHIs ([Roth 2007; Santamouris 2015](#)), dry seasons typically have the largest UHIs and thus would pose the most heat-based health risk to Lagos. However, because tropical environments experience seasonality in UHIs, our results may differ in Lagos's wet season for which further exploration is needed.

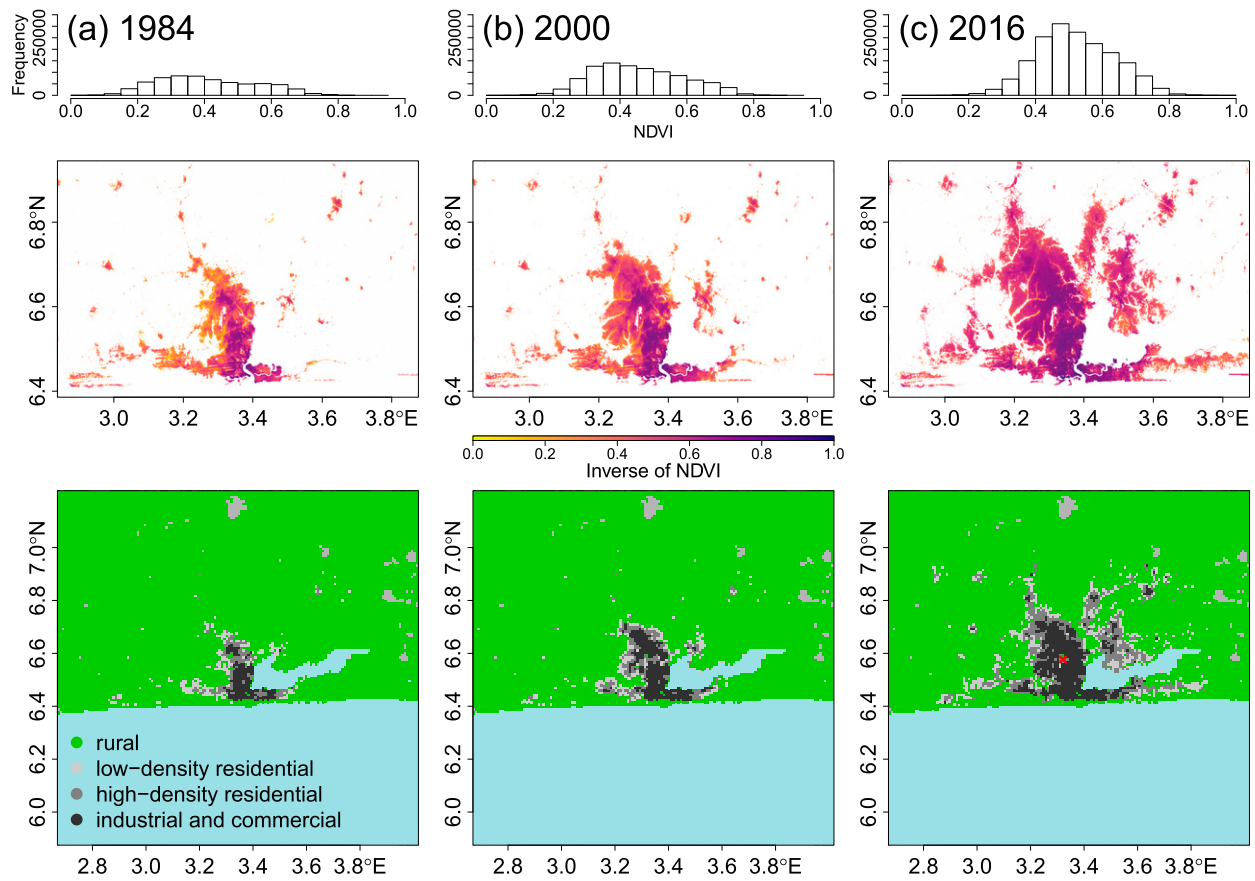


FIG. 2. For (a) 1984, (b) 2000, and (c) 2016, (top) histograms using the inverse NDVI as a proxy for the rapid urbanization for the three cases, (middle) as in the top row but shown spatially, and (bottom) WRF inner domain land use in Lagos. The red cross in the 2016 land-use case denotes the location of the Lagos Airport observations.

Initial and boundary conditions were provided by using NCEP Final Operational Model Global Tropospheric Analyses data at  $1^{\circ}$  horizontal and six-hourly temporal resolution (NOAA/NCEP 2000). To represent the physical urban

processes in Lagos, the Single-Layer Urban Canopy Model (SLUCM) was used (Kusaka et al. 2001). Of the urban schemes coupled to WRF, SLUCM represents medium complexity and is used globally in WRF-urban studies (e.g., Kusaka et al. 2012;

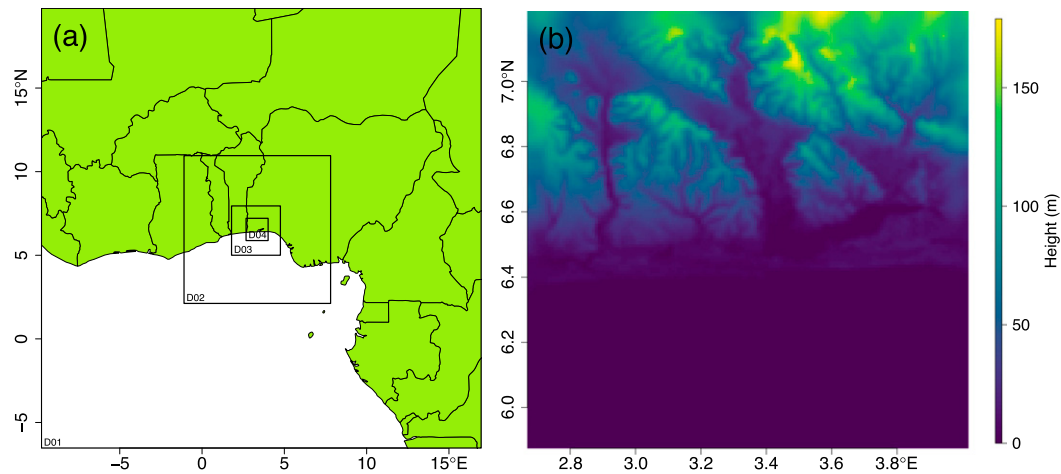


FIG. 3. (a) WRF Model nests extending horizontally 112, 112, 112, and 151 grid cells, at 27-, 9-, 3-, and 1-km resolution, respectively. (b) Topography inside the innermost domain D04.

TABLE 1. WRF multiphysics options and RMSE evaluation at Lagos Airport. Model run A used default WRF land use and parameters, run B used updated land use, and run C used updated land use and parameters. Model runs D–N use the updated land use and parameter configuration from run C.

Model run	Boundary layer		Microphysics		Shortwave radiation			RMSE	
	MYJ	BouLac	Thompson	WSM3	Dudhia	Goddard	RRTMG	Temperature	Wind speed
A	x		x				x	1.57	0.99
B	x		x			x	x	1.34	1.04
C	x		x			x	x	1.07	0.99
D		x	x				x	1.00	1.46
E	x		x			x		1.07	1.01
F		x	x			x		1.02	1.53
G	x		x		x			1.57	0.91
H		x	x		x			1.15	1.26
I	x			x			x	1.08	0.99
J		x		x			x	0.99	1.47
K	x			x		x		1.08	1.01
L		x		x		x		1.00	1.51
M	x			x	x			1.59	0.91
N		x		x	x			1.16	1.25

(Li et al. 2013; Loridan et al. 2013; Chen et al. 2014; Doan and Kusaka 2016). The SLUCM contains a two-dimensional urban street canyon with heat fluxes calculated for each surface (roofs, walls, and roads) and their interaction within the street canyons (building shadowing, reflecting, and trapping). Building-morphology parameters (used by SLUCM) more closely aligned to Lagos (Jackson et al. 2010) were used. Despite a citywide anthropogenic heat flux estimated for Lagos (Sailor et al. 2015), because of a lack of spatial and diurnal anthropogenic data, values were kept as default. These were 20, 50, and 90  $\text{W m}^{-2}$  for the three urban categories, with a diurnal weighting corresponding to morning and afternoon rush-hour times. Moving through time, we are only able to account for anthropogenic heat changes through areas becoming more urbanized (represented by the NDVI) and therefore modeled in a different urban land-use class. The model time step was set at 90 s.

WRF contains an extensive set of physics options representing processes such as cloud ice nucleation. However, a configuration “rule” does not exist for different WRF applications and locations. We chose to conduct a multiphysics evaluation to find a WRF configuration suitable for Lagos using a combination of options: two boundary layer options, MYJ (Janjić 1994) and BouLac (Bougeault and Lacarrere 1989); two cloud microphysics options, Thompson (Thompson et al. 2008) and WSM3 (Hong et al. 2004); and three shortwave radiation physics options, RRTMG (Iacono et al. 2008), Goddard (Chou and Suarez 1999), and Dudhia (Dudhia 1989). Note that this is not an exhaustive list of physics options but rather is a small subset that was chosen on the basis of selections made in previous WRF-urban studies (Loridan et al. 2013). We performed an additional control run to compare the default model land use with our satellite-derived land use. These 14 configurations are listed in Table 1. Each simulation was principally compared with meteorological records at Lagos Murtala Muhammed Airport (hereinafter referred to as Lagos Airport; latitude 6.57°N, longitude 3.32°E, and elevation

41 m). The Lagos Airport station data were available from the NOAA Integrated Surface Database (<https://www.ncdc.noaa.gov/isd>) and form part of a growing observation network by the Nigerian Meteorological Agency (Hussaini and Yakubu 2019). Note that the comparison is affected by the different spatial scales captured by the model and point observations. The evaluation covers the same period as the one on which we conducted our analysis in February 2016.

Overall, the multiphysics runs for 2-m air temperature showed good agreement with the observations (see top row of Fig. 4a). However, all runs underpredict peak daytime temperatures, by up to 5.18°C on occasion. We also find considerable variability [standard deviation (std dev) of 0.59°C] between the different physics configurations, as seen in the top row of Fig. 4b.

For wind speeds, there is no information on the height at which the observations are taken. A comparison assuming a 10-m mast shows a large model overestimation. However, if modeled wind speeds are reduced to a 3-m height using the following wind profile power law,

$$\frac{V}{V_r} = \left( \frac{Z}{Z_r} \right)^\alpha,$$

where  $V$  is wind speed,  $Z$  is height, and the exponent  $\alpha$  is set for a city at 0.32 (Cook 1997), we find good agreement between observed and predicted values (see bottom row of Fig. 4a). Note that values of zero for wind speed are removed, with the assumption being that these are likely due to the anemometer stall speed. Similar to temperature, considerable variability is found between the multiphysics runs (std dev of 0.49  $\text{m s}^{-1}$ ). The distributions of wind speeds between multiphysics configurations are provided in the bottom row of Fig. 4b.

The root-mean-square error (RMSE), a commonly used statistical measure for model comparison, is chosen to evaluate each multiphysics run. The RMSE results are shown in Table 1. Here, model run A used default WRF land use and parameters,

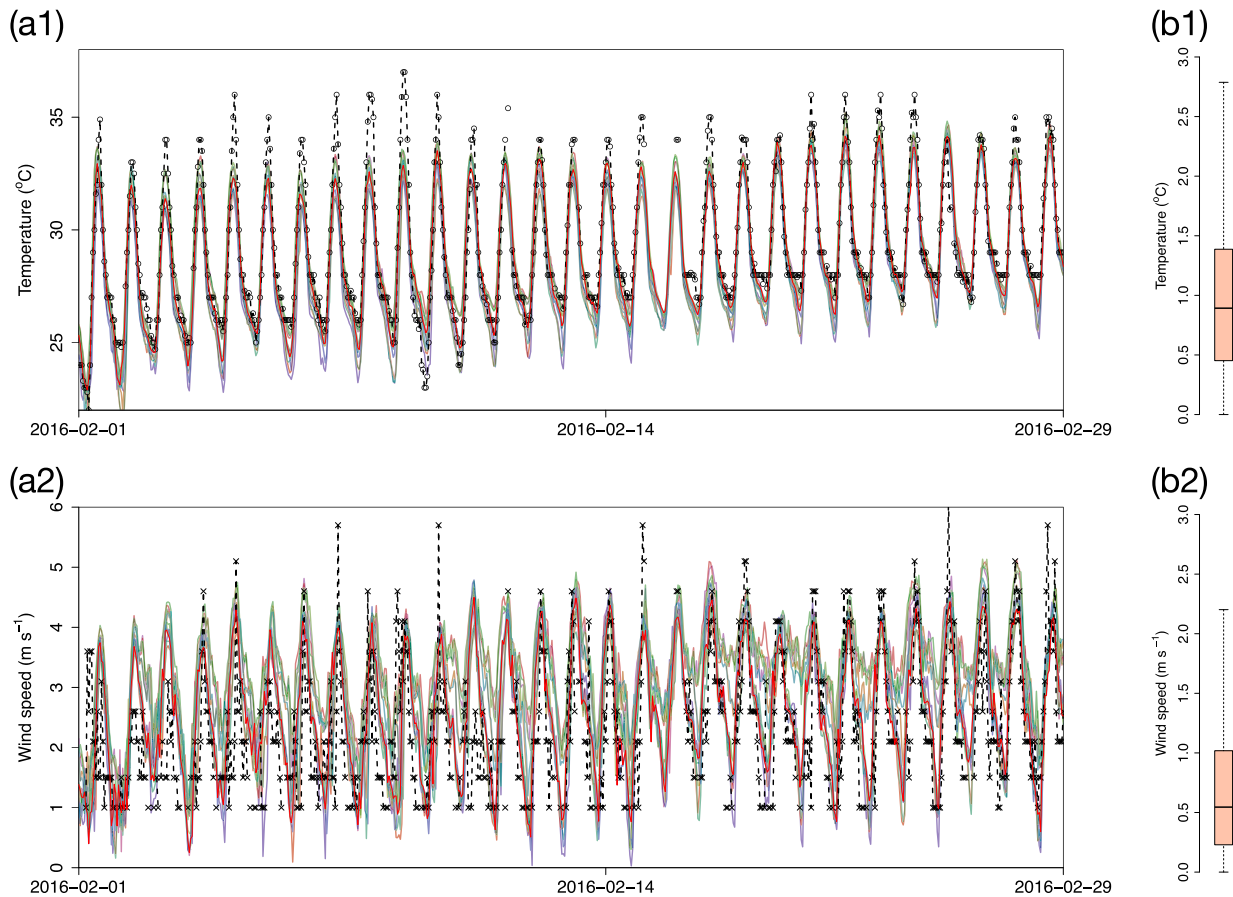


FIG. 4. Multiphysics evaluation results for (a1) temperature and (a2) wind speed. The solid lines are the modeled results, and the dashed line with points is the observations at Lagos Airport. In each plot, the solid red line is the model configuration that we take forward into the IMV ensemble. Also shown are the distributions from the multiphysics runs for (b1) temperature and (b2) wind speed.

run B used updated land use (detailed in section 2a), and run C used updated land use and more specific urban parameters from Jackson et al. (2010). Model run C, with updated land use and parameters, was then used as a basis for the remaining multiphysics evaluation runs (D–N). The RMSE results show a 0.2°C reduction through implementing updated land use (see model run A vs B in Table 1) and 0.5°C reduction by using both updated land use and parameters (see model run A vs C in Table 1). Considering that the default WRF land use is outdated (derived from 2001 MODIS satellite imagery), and that Lagos is rapidly expanding, these results are not surprising.

For each multiphysics combination, nighttime RMSE for temperature was lower across the board than during daytime. While we should not ignore daytime performance, modeling nighttime temperatures with low error is important for this study because the UHI is predominantly a nighttime phenomenon. We note that the physics combinations that created the lowest RMSE for temperature did not always perform as well for wind (see Table 1). To take the best configuration forwards into the Lagos ensemble, to account for internal model variability (detailed in the following section), the RMSE results were normalized for temperature and wind speed, with the resulting normalized RMSE values totaled

for each variable. We then took the model with the lowest total normalized RMSE as the best all-rounder. Wind performance was taken into equal consideration because of its modulating influence on the UHI intensity. Coincidentally, the best multiphysics option was the default configuration, albeit with updated land use and parameters. While we were able to improve the model performance at Lagos Airport, we acknowledge that limited data means evaluation was only possible for a small portion of the model.

Additional model checks were made at a station outside of Lagos, Ijebu-Ode (latitude 6.83°N, longitude 3.93°E, and elevation 77 m). Note that data were only available every 3–6 h; February 2016 contained 123 data points as compared with 654 at Lagos Airport. For the final WRF configuration, RMSE for air temperature was 2°C and for wind speed was 1.3 m s<sup>-1</sup> at Ijebu-Ode. Higher RMSE when compared with the Lagos Airport station is likely due to two contributing factors: (i) the model land-use specification at Ijebu-Ode being rural whereas it is actually low-density urban (this inaccuracy is due to our updated satellite-derived land use being created only for Lagos, i.e., excluding Ijebu-Ode) and/or (ii) the location of the station at the edge of the inner model domain, meaning it may not

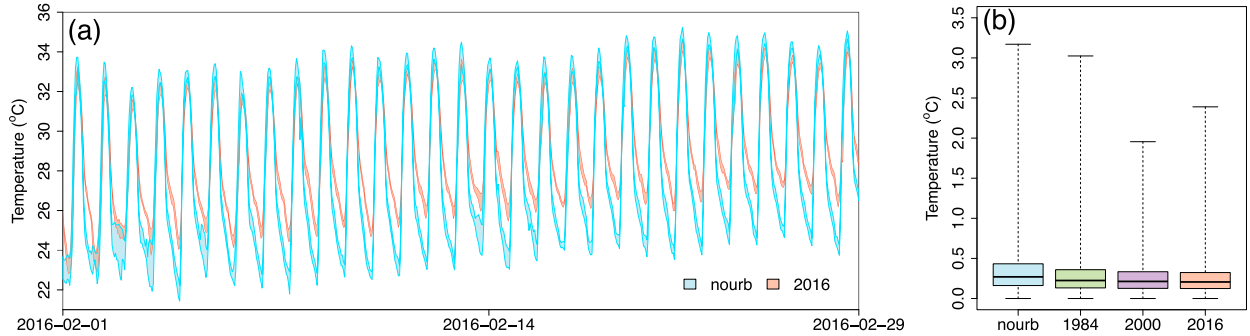


FIG. 5. (a) Temperature range between all ensemble members at Lagos Airport for the 2016 (red shading) and NOURB (blue shading) cases. (b) Boxplot showing the IMV spread at Lagos Airport for all cases during the time period shown in (a). The whiskers denote the maximum and minimum range.

be completely in equilibrium because of smoothing processes to the parent domain.

#### c. Ensemble configuration

Internal model variability may cause differences in results due to nonlinear processes within regional climate models (Laux et al. 2017; Lucas-Picher et al. 2008; Bassett et al. 2020). Therefore, we need to be confident that any warming in our results due to urbanization exceeds effects caused by internal model variability (IMV). Based on previous research to the number of ensemble members to capture the majority of IMV (Bassett et al. 2020), we created a 35-member ensemble for each of the land-use cases detailed above. All members were run on a local high-performance computer, although we are additionally exploring the benefits of cloud-computing technology to facilitate future access to models like WRF and increase processing power (Simm et al. 2018).

The ensemble members were started at 42-h intervals covering a 2-month period (1 December 2015–31 January 2016). Aside from start time, each member used identical boundary conditions during the analysis period. Once all members were running, we continued the simulations for a 1-month analysis period (1 February 2016–29 February 2016) using the same boundary conditions for each member in each case. Figure 5 shows an example of the impacts of IMV, that is, the range in predicted temperatures, at the grid cell located over Lagos Airport.

#### d. Analysis methods

The UHII is derived as the difference in temperature between each urban (1984, 2000, and 2016) case and the NOURB case for 2-m modeled air temperatures. To show the significance of the UHII response due to urbanization, we take a similar approach to Laux et al. (2017) and calculate the signal-to-noise ratio (SNR)—that is, the size of the response to urbanization relative to the internal model variability:

$$\text{SNR} = \frac{\text{etm}A - \text{etm}B}{\text{std dev}A + \text{std dev}B},$$

where etm is the ensemble time mean and std dev is the standard deviation for a given case *A* and the preceding case *B* (e.g., 1984 – NOURB).

### 3. Results and discussion

#### a. Lagos urbanization and heat island growth

The intense urbanization between 1984 and 2016 is shown in Fig. 2. The growth of Lagos during this period was largely constrained to a northeast direction by the adjacent natural features: the Gulf of Guinea, Lagos Lagoon, and surrounding wetlands. Within the study domain (151 km wide) we find the land surface covered by urban regions to increase from 720 km<sup>2</sup> in 1984 to 1009 km<sup>2</sup> and 2053 km<sup>2</sup> in 2000 and 2016, respectively. While this rate of expansion is faster than an earlier estimate of Lagos's city expansion (Barredo and Demicheli 2003), it is not uncommon for a megacity, and similar expansion rates have been found for Delhi (Mohan et al. 2011) Mumbai (Moghadam and Helbich 2013) in India and Shanghai, China (Yin et al. 2011).

Figure 6a shows the resulting urbanization-induced warming. Within the urban outlines for each case (1984, 2000, and 2016), a nocturnal (based on daily sunrise and sunset times) spatial etm UHII of 0.83° (std dev of 0.62°C), 1.04° (std dev of 0.71°C), and 1.27°C (std dev of 0.78°C) were modeled, respectively (all results are presented in this order from here on). The standard deviation values in parentheses are the combined spatial, temporal, and ensemble distribution for Lagos's UHI; this distribution is shown in Fig. 7. At an hourly time resolution, the ensemble-mean nocturnal UHII peaks at 3.19°, 3.67°, and 4.13°C, respectively. In Fig. 6c we show a nocturnal UHI transect through the city, from the southwest to northeast for each case to further emphasize these impacts of urbanization. We clearly see both Lagos's sizable warming, particularly moving from 1984 to 2016 in regions of urban growth, as well as the advected warmth from the city to rural regions, for example, around cell 100, and as detailed below.

In addition, we find that Lagos exhibits a slight urban cool island (UCI) during the day (see distributions in Fig. 7a). The magnitude of this UCI is significantly less than the nocturnal UHI, and unlike the nocturnal UHI we do not find much difference between daytime UCI intensities. Daytime spatial etm UCIs inside Lagos's urban limits for each case are −0.26° (std dev of 0.66°C), −0.24° (std dev of 0.70°C), and −0.22°C (std dev of 0.76°C). UCIs may form because of

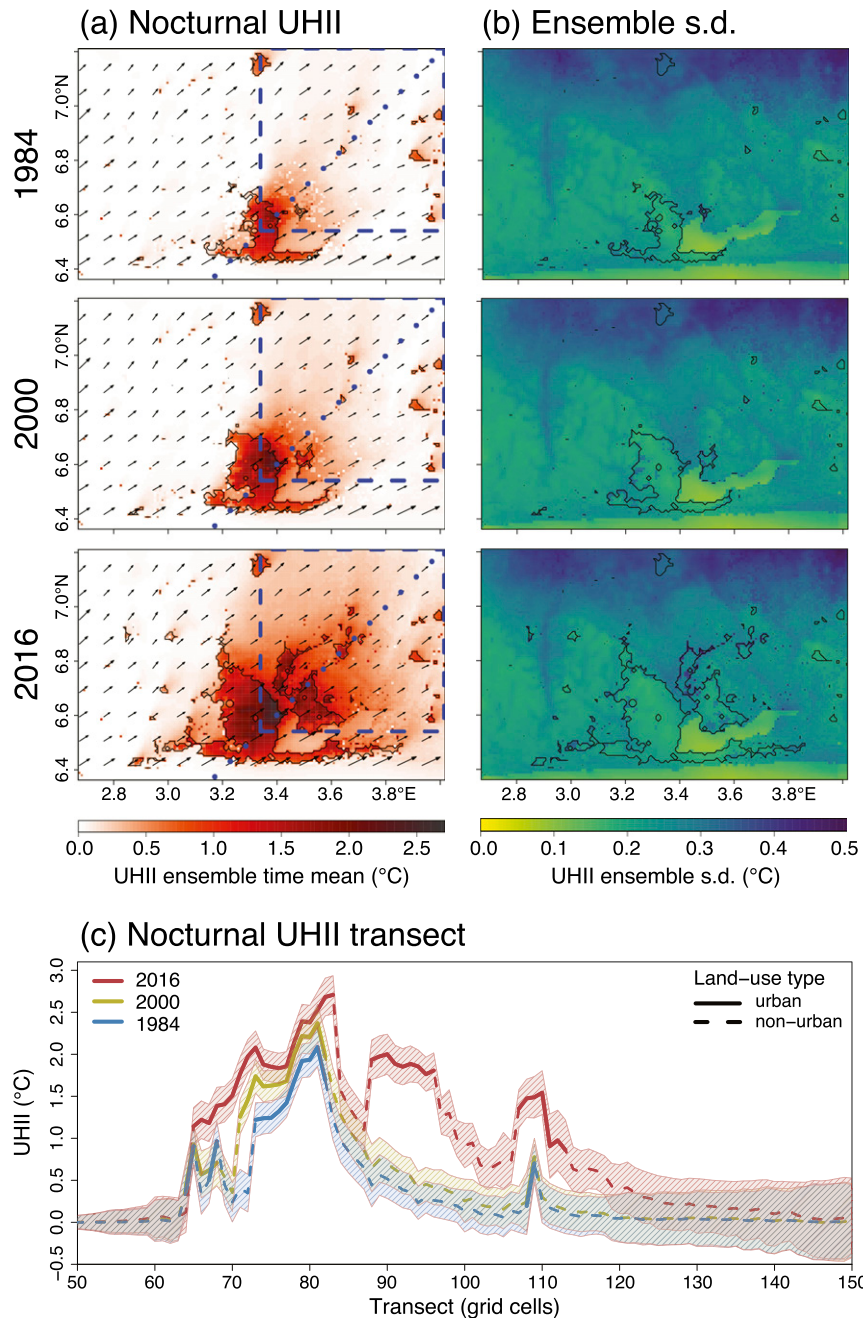


FIG. 6. (a) Nocturnal etm UHII. Arrows are the etm 10-m wind speed and direction. The dash-outlined blue box represents where urban heat advection is quantified. The arrows are mean wind direction and speed (maximum of  $6.02 \text{ m s}^{-1}$  at night). (b) Standard deviation of the ensemble members only (i.e., not diurnal variation). (c) Nocturnal southwest–northeast transect across the path shown by the dotted blue line in (a). The shading represents  $\pm 1$  standard deviation of the ensemble along the transect [in (b)]. The solid lines represent urban land use, and dashed lines represent nonurban land use.

differences between urban and rural boundary layer heights in the morning, that is, shallower rural boundary layers warm quicker (Theeuwes et al. 2015). Considering that the UHI is predominantly a nighttime feature and is significantly

more pronounced than the UCI, hereinafter the focus is on nighttime only.

Although Lagos's spatial etm UHII intensification of  $0.44^\circ\text{C}$  across a 32-yr period appears to be modest, this is (i) larger

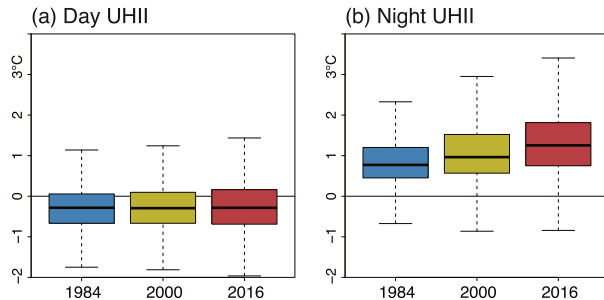


FIG. 7. (a) Daytime and (b) nighttime UHII box plots containing all spatial, temporal, and ensemble values within the 1984, 2000, and 2016 urban outlines. Whiskers are  $1.5 \times$  interquartile range.

than the observed climate change magnitude of approximately  $0.12^{\circ}\text{C decade}^{-1}$  (NOAA/NCEI 2019) and (ii) covers a rapidly growing area. In 1984, we simulate an area of  $254 \text{ km}^2$  where spatial etm UHII exceed  $1^{\circ}\text{C}$ , expanding to  $522 \text{ km}^2$  in 2000, and to  $1572 \text{ km}^2$  in 2016. Similarly, areas of UHII exceeding  $2^{\circ}\text{C}$  rise from 6 to 45 and then to  $186 \text{ km}^2$ . We also note the maximum gridcell etm nocturnal UHII values of  $2.28^{\circ}$ ,  $2.49^{\circ}$ , and  $2.7^{\circ}\text{C}$  in urban regions downwind of the city center, caused by a process known as urban heat advection (Bassett et al. 2016; Bohnenstengel et al. 2011). The analysis period in February 2016 contains a dominant southwesterly wind direction, reflected in the location of maximum UHII.

Our results also show that warmth from Lagos is advected far outside the city limits; see northeast sectors in Fig. 6a and the transect in Fig. 6c. Extending approximately the length scale of the city for each case, this phenomenon is rarely considered in UHI impact studies. For simplicity we overlay a square on the northeast sector of the domain (see dashed outline in Fig. 6a). Here the etm nocturnal rural warming (excluding urban and water bodies) is  $0.10^{\circ}\text{C}$  (std dev of  $0.35^{\circ}\text{C}$ ),  $0.15^{\circ}\text{C}$  (std dev of  $0.40^{\circ}\text{C}$ ), and  $0.39^{\circ}\text{C}$  (std dev of  $0.51^{\circ}\text{C}$ ). The maximum warming due to advection from the city occurs in grid cells directly adjacent to the city with an etm up to  $1.83^{\circ}\text{C}$ . We find that the rural-only area impacted by warmth from Lagos that exceeds an etm value of  $0.5^{\circ}\text{C}$  expands from  $183 \text{ km}^2$  in 1984 to  $399 \text{ km}^2$  in 2000 and to  $1558 \text{ km}^2$  in 2016.

The ensemble-only UHII variability is shown in Fig. 6b. Here the standard deviation within each urban outline is  $0.23^{\circ}\text{C}$ ,  $0.23^{\circ}\text{C}$ , and  $0.24^{\circ}\text{C}$  for the three cases. Spatially, levels of variability change across the modeled domain, and spatial differences in internal model variability have also been reported for simulations of other regions (Jerez et al. 2013). We find the lowest variability over the oceans, and generally lower values across the urban areas when compared with rural areas. We also note an association between the ensemble variability and topography features within the domain (see Fig. 3b). Because the focus of our study is the warming resulting from rapid urbanization, we do not attempt to disentangle causes for spatial internal model variability. However, we suggest that in addition to topography these could be a function of land-use type and distance from domain boundaries. Further, to uncertainty caused by internal model variability, our simulations

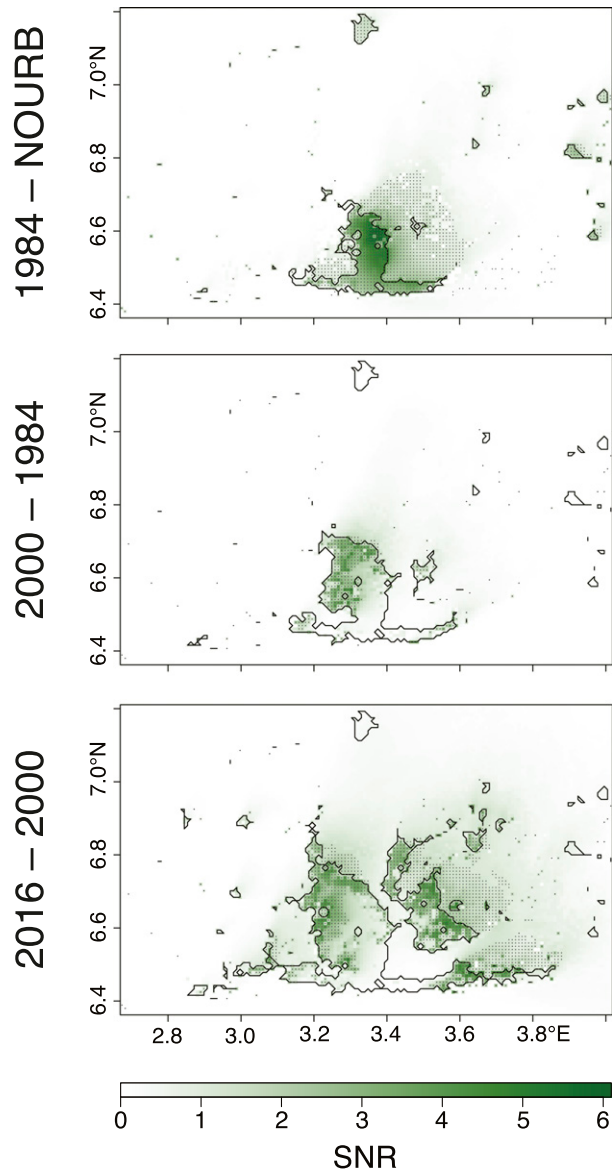


FIG. 8. SNR comparing each urban case with the preceding case. The black dots indicate where the differences are significant at the 1% level (two tailed  $t$  test, adjusted to account for the false discovery rate).

also contain unquantifiable structural uncertainty due to a lack of observations for evaluation.

The statistical significance of the results is shown in Fig. 8. Here the expansion of the city is seen through areas of high SNR values in each case. Although there is large expansion of urban land use moving from 2000 to 2016, we see lower SNR values compared to moving between the NOURB and 1984 cases. This is due to new areas of urban growth situated in areas already warmed by urban heat advection from the previous case, meaning that the signal is less pronounced. The significance of Lagos's urbanization is additionally checked by performing an unpaired  $t$  test at each grid cell, and Fig. 8 indicates

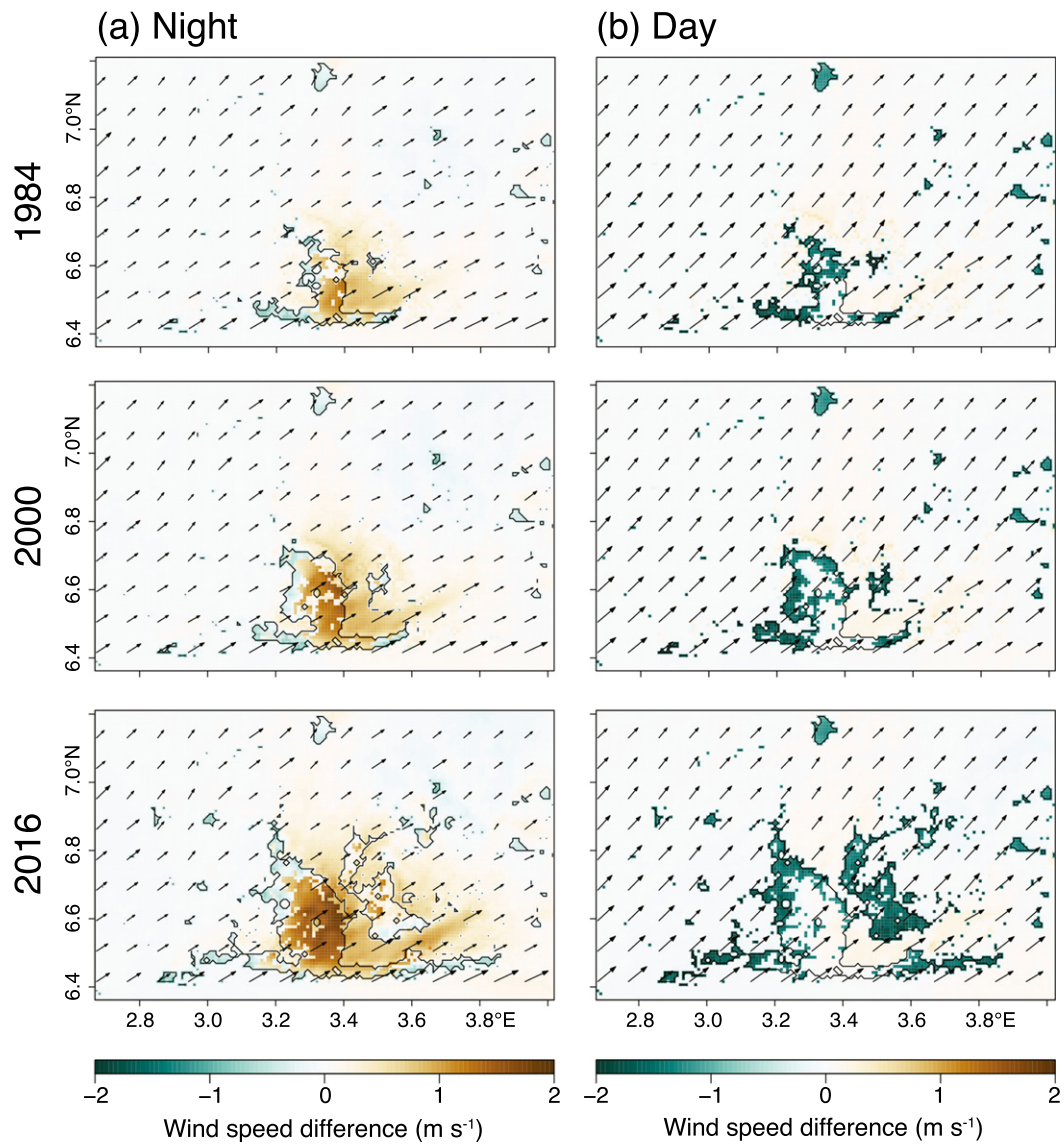


FIG. 9. Etm wind speed differences between each urban (1984, 2000, and 2016) case and the NOURB case for (a) night and (b) day.

where  $p < 0.01$ , adjusted to account for false discovery rates since we are examining multiple grid cells (Benjamini and Hochberg 1995). Grid cells that have significant differences in means between each successive case correspond to areas of higher SNR. We infer from both tests that the impact of Lagos's urbanization exceeds any model IMV.

#### b. Secondary impacts of the UHI in Lagos

While temperature is the most noticeable impact of rapid urbanization, small perturbations caused by Lagos's UHI are found in other simulated meteorological variables, particularly surface-level winds and boundary layer heights (depth of the bottom layer of the atmosphere).

At night, mostly increased wind speeds are found, particularly in the city center and areas downwind of the city. Areas of

decreased wind speeds, however, are found to the north and west areas in the city for each case (see Fig. 9a). We find maximum etm wind speed increases of 1.32, 1.72, and  $1.95 \text{ m s}^{-1}$  for 1984, 2000, and 2016. We also note from Fig. 9a that increased wind speeds are not constrained to the city and are also found in areas immediately downwind of the city, similar to areas of advected urban heat shown earlier. For the daytime case we find a similar spatial pattern to the nighttime, except no changes in wind speed are present in areas of nighttime increases, and larger reductions in wind speed are found in areas also containing nighttime decreases. Overall, we find a daytime mean wind speed reduction of approximately  $1 \text{ m s}^{-1}$  (std dev of  $1 \text{ m s}^{-1}$ ) within the urban outline for each case. Actual wind speeds for each case are provided in Fig. S1 in the online supplemental material. Similar to the internal

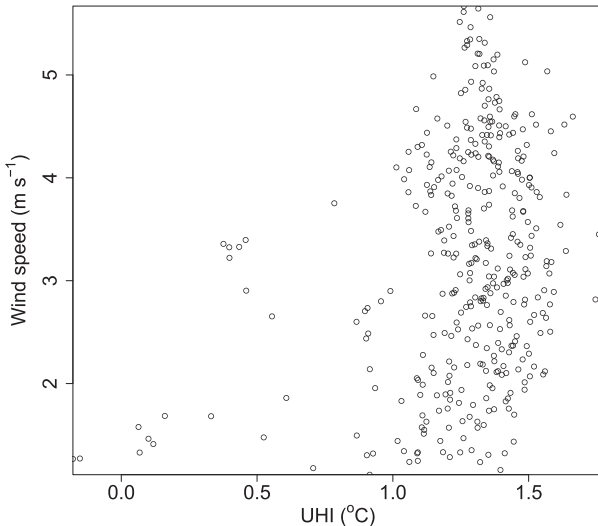


FIG. 10. Relationship between the hourly nighttime ensemble spatial mean wind speed and UHI within the 2016 urban outline.

model variability for the UHII, differences between ensemble members for wind speeds differences exist. We find a wind speed difference standard deviation of approximately  $0.4 \text{ m s}^{-1}$  at night and  $0.55 \text{ m s}^{-1}$  during the day in each urban case. We also generally see lower variability for wind over urban areas. Spatial variability maps for wind are provided in Fig. S2 in the online supplemental material; in Fig. S2 it is seen that, during the day, higher variability in the top regions of the domain is particularly notable.

Increased drag from urban buildings explains slower wind speeds found during the day and in certain areas at night. Increased wind speeds at night found in the city center and downwind areas in all cases may be explained by UHI-induced temperature and pressure gradients (Haeger-Eugensson and Holmer 1999; Wang and Li 2016; Droste et al. 2018). Effectively, rising warm air from Lagos leaves an area of lower pressure that drives inward flows, with this phenomenon overcoming any friction-related wind speed decreases. The relationship between mean wind speed and UHII for the 2016 case is shown in Fig. 10, where an increase in UHII is found with increasing wind speed (correlation coefficient  $r = 0.28$ ; significance level  $p < 0.01$ ). Albeit weak, this relationship is contradictory to the pattern usually found where UHIs are modulated by wind, with lower speeds resulting in higher UHIs due to less turbulent mixing (Morris et al. 2001). Aside from a daily wind speed pattern (see wind time series on the bottom row of Fig. 4a), wind shows little variability between each day of the analysis period; therefore, there is not enough nighttime variation in the modeled wind speed data to find the typical UHI wind speed relationship. Instead Fig. 10 shows that the UHI is enhancing wind speeds. This relationship may have a self-regulating effect on the UHI that warrants further investigation, that is, increased advection of cooler rural air to the city.

UHIs are known to increase boundary layer heights at night due to increased levels of heat propagating vertically (Pal et al. 2012). Relative to the NOURB case boundary layer height of

approximately 370 m, we find etm height increases of 86 (std dev of 143 m), 104 (std dev of 151 m), and 125 m (std dev of 161 m) at night over the city (Fig. 11a). During the day we find slight height reductions (Fig. 11b). Boundary layer heights for each case and the standard deviation created by the ensemble are provided in Figs. S3 and S4, respectively, in the online supplemental material. At night, the largest height increases are found in the northeast sectors of the city (similar to the UHI pattern discussed above), and extend into the immediately adjacent downwind rural areas, up to  $\sim 5 \text{ km}$  for the 2016 case.

A transition to reduced boundary layer heights are modeled downwind of areas of increased boundary layer heights (see area northeast of Lagos in Fig. 11a). Boundary layer height reductions extend to approximately the length scale of the city and are not present at upwind locations nor are they as large as the increases in heights over the city. Downwind reductions in boundary layer heights are also present in the daytime cases, although there is less spatial consistency to the pattern. To quantify the downwind boundary layer height reduction, we crop the domain to the northeast sector, with nonurban land use only. Furthermore a  $5 \times 5$  gridcell buffer was removed northeast of any urban grid cell to account for the transition from increased to decreased heights. Within the northeast sector of the domain, the overall etm reduction in boundary layer heights of 9 (std dev of 127 m), 16 (std dev of 133 m), and 22 m (std dev of 141 m) are found. SNR values for the boundary layer height reduction and  $t$  test comparing NOURB to 2016 are provided in Fig. 12. Although the SNR values are lower than found for UHII and mean boundary layer reductions appear small, they occur over a downwind area of approximately  $3000 \text{ km}^2$ , or larger considering the effect extends to the domain edge. Cautiously, while we note this feature in our results, modeled boundary layer heights are sensitive to the choice of boundary layer schemes (Kim et al. 2013). Although reduced boundary layer heights downwind would be difficult to observe because of a lack of downwind vertical observations from cities, this feature has been theorized to be caused by the outflow of warm urban air (in an urban plume) thus suppressing downwind boundary layer heights (Barlow 2014). This theory is supported by idealized modeling (Zhang et al. 2014).

#### 4. Conclusions

Lagos is one of the fastest-growing cities in the world, tripling in size over 1984–2016. This has social and environmental impacts, yet excess heat caused by the urban heat island effect has not been well explored in the Global South, reflecting a broader paucity of environmental measurement and modeling studies. Due to sparse data availability, we explored UHI effects in Lagos using an ensemble approach with the WRF numerical model. Overall, our results indicate that (i) the area influenced by the UHI effect is increasing steeply, (ii) within Lagos's urban outline the UHI intensity (UHII) is increasing, and (iii) rural areas downwind are being warmed by the city. Although we accounted for internal model variability, model evaluation was only possible at a single location owing to limited observations in the region. Although we are confident

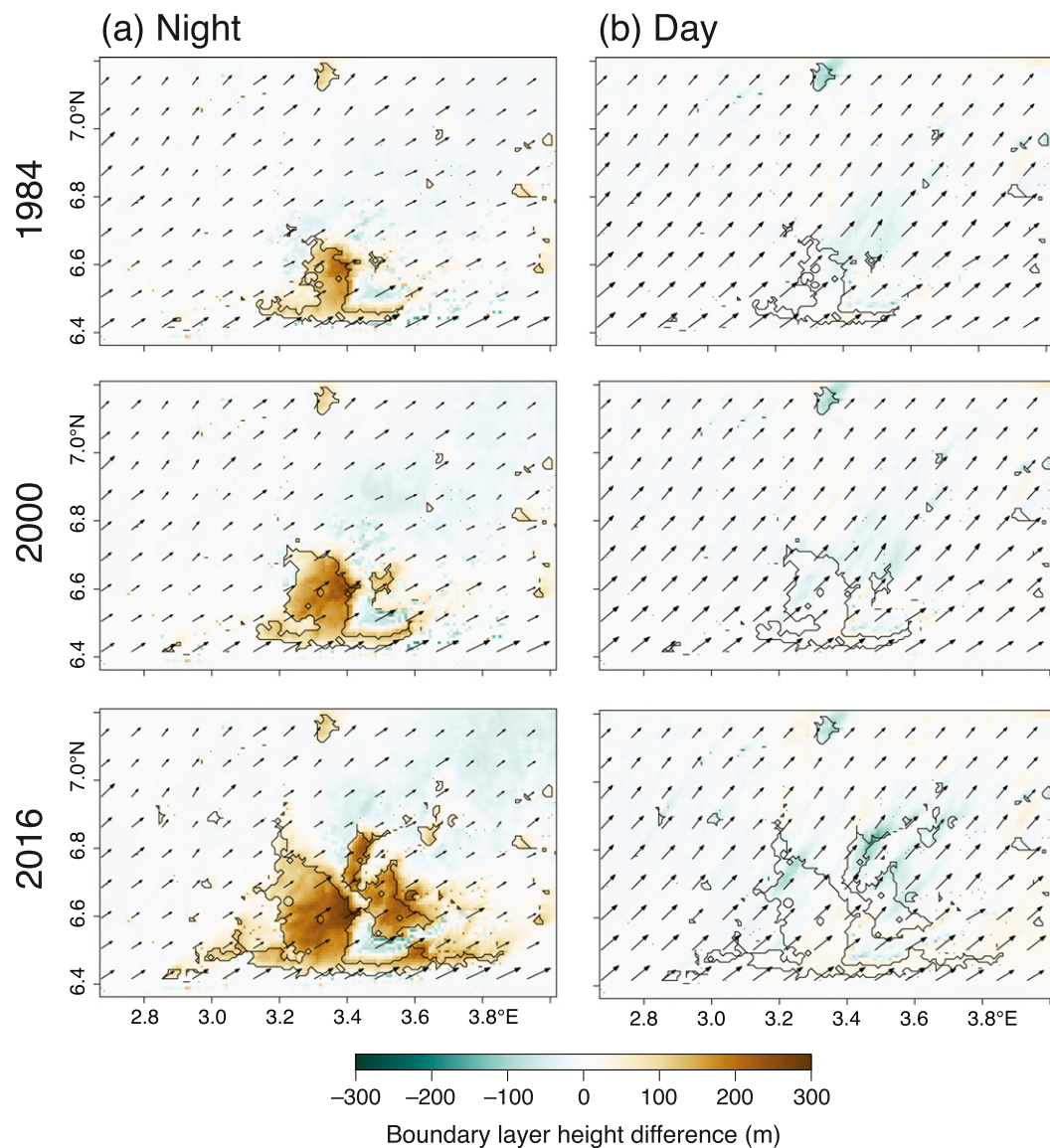


FIG. 11. Etm boundary layer height differences between each urban and the NOURB case for (a) day and (b) night.

in the sign of our results, the precise effects of urbanization in Lagos may not be fully realized.

Nighttime ensemble-time-mean (etm) UHII increased  $0.44^{\circ}\text{C}$  between 1984 and 2016 using a fixed, monthlong set of meteorological conditions for each case. At an hourly scale, maximum modeled UHII values increased between 1984 and 2016 by  $0.94^{\circ}$  to  $4.13^{\circ}\text{C}$ . The true scale of the impact is seen spatially, where the area in which etm UHIIs exceed  $1^{\circ}\text{C}$  was found to steeply increase. The largest UHIIs were found to the northwest of the city for each case, caused by a dominant southwesterly wind that also advected the city's warmth into downwind rural areas. While increased nighttime temperatures are most commonly associated with urbanization, we also found modification to boundary layer heights and surface-level winds. Of particular interest was the decreased boundary layer heights downwind of Lagos. Although

small in magnitude compared to daytime boundary layer height increases over the city, this has potential implications for rural communities near Lagos, for example, potential worsening of air quality due to the shallower mixing layer.

Despite accounting for internal model variability by using a WRF ensemble, our approach is limited by a lack of data for configuration and evaluation (although a favorable comparison against temperature and wind observations at Lagos Airport was found). To illustrate the UHI under more extreme conditions, our simulations were conducted against a background of an unusually warm recent period, yet the UHII will be sensitive to the prevailing meteorology. Our results represent Lagos's dry season only and further exploration is needed to map seasonal changes in UHI intensities. Notwithstanding, the modeling results in this paper suggest a significant,

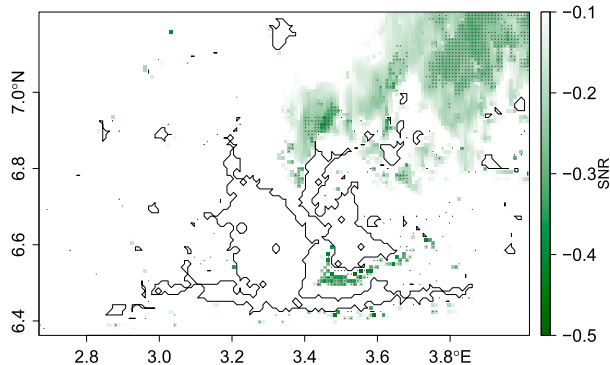


FIG. 12. SNR between the NOURB and 2016 cases. The black dots are grid cells for which the  $t$  test rejects the null hypothesis, i.e., there is a significant difference between the means of each case (adjusted  $p < 0.01$ ). Note that only negative SNR values are shown to highlight confidence in areas of boundary layer height reduction.

urbanization-driven warming of Lagos's local climate of  $0.15^{\circ}\text{C decade}^{-1}$ , 25% faster than climate change, which is happening in addition.

With temperatures projected to increase in this region for all future climate scenarios (IPCC 2013), combined with this rapid UHI growth, there is a clear need to better understand the future heat of cities like Lagos, to better inform their adaptation and mitigation needs. However, despite efforts to increase observational capacity in Nigeria (Hussaini and Yakubu 2019), the paucity in observational data remains a challenge. We hope that these results may be used to support local studies on the changing environment and help prioritize new observations in a rapidly warming area that is already home to tens of millions of people and that may triple in size again by the end of this century.

**Acknowledgments.** This research was made possible through the UK EPSRC Grant EP/N027736/1: Models in the Cloud and use of the High End Computing (HEC) HPC at Lancaster University (<https://www.lancaster.ac.uk/iss/hec/HEC-flyer.pdf>). We extend our gratitude to the WRF community for open access to their model, in addition to the National Centers for Environmental Prediction and Centre for Environmental Data Analysis for provision of data. WRF Model control files (“namelist”) for our configuration are available from the authors. In addition, we thank the wider “Ensemble” research team (<https://www.ensembleprojects.org/>) for their guidance.

**Data availability statement.** The source code and documentation for the WRF Model are available online (<http://www2.mmm.ucar.edu/wrf/users/>). The Landsat satellite images used in this study can be retrieved from the USGS (<http://earthexplorer.usgs.gov>). The NCEP FNL Operational Model Global Tropospheric Analyses are available online (<https://doi.org/10.5065/D6M043C6>). All WRF configuration files and model outputs that support the findings of this study are available from the corresponding author upon reasonable request.

## REFERENCES

- Adeloye, A. J., and R. Rustum, 2011: Lagos (Nigeria) flooding and influence of urban planning. *Proc. Inst. Civ. Eng. Urban Des. Plann.*, **164**, 175–187, <https://doi.org/10.1680/udap.1000014>.
- Ajibola, M. O., B. A. Adewale, and K. C. Ijasan, 2012: Effects of urbanisation on Lagos wetlands. *Int. J. Bus. Soc. Sci.*, **3**, 310–318.
- Alens, O. P., 2014: Meteorological services for disaster risk prevention and mitigation in Nigeria. *J. Environ. Earth Sci.*, **4**, 66–76.
- Ayanlade, A., and O. O. Jegede, 2015: Evaluation of the intensity of the daytime surface urban heat island: How can remote sensing help? *Int. J. Image Data Fusion*, **6**, 348–365, <https://doi.org/10.1080/19479832.2014.985618>.
- Azevedo, J. A., L. Chapman, and C. L. Muller, 2016: Urban heat and residential electricity consumption: A preliminary study. *Appl. Geogr.*, **70**, 59–67, <https://doi.org/10.1016/j.apgeog.2016.03.002>.
- Barlow, J. F., 2014: Progress in observing and modelling the urban boundary layer. *Urban Climate*, **10**, 216–240, <https://doi.org/10.1016/j.uclim.2014.03.011>.
- Barredo, J. I., and L. Demicheli, 2003: Urban sustainability in developing countries' megacities: Modelling and predicting future urban growth in Lagos. *Cities*, **20**, 297–310, [https://doi.org/10.1016/S0264-2751\(03\)00047-7](https://doi.org/10.1016/S0264-2751(03)00047-7).
- Bassett, R., X. Cai, L. Chapman, C. Heavyside, J. E. Thorne, C. L. Muller, D. T. Young, and E. L. Warren, 2016: Observations of urban heat island advection from a high-density monitoring network. *Quart. J. Roy. Meteor. Soc.*, **142**, 2434–2441, <https://doi.org/10.1002/qj.2836>.
- , P. J. Young, G. Blair, F. Samreen, and W. Simm, 2020: A large ensemble approach to quantifying internal model variability within the WRF numerical model. *J. Geophys. Res. Atmos.*, **125**, e2019JD031286, <https://doi.org/doi.org/10.1029/2019JD031286>.
- Benjamini, Y., and Y. Hochberg, 1995: Controlling the false discovery rate: A practical and powerful approach to multiple testing. *J. Roy. Stat. Soc.*, **57B**, 289–300, <https://doi.org/10.1111/j.2517-6161.1995.tb02031.x>.
- Bohnenstengel, S. I., S. Evans, P. A. Clark, and S. E. Belcher, 2011: Simulations of the London urban heat island. *Quart. J. Roy. Meteor. Soc.*, **137**, 1625–1640, <https://doi.org/10.1002/qj.855>.
- Bougeault, P., and P. Lacarrere, 1989: Parameterization of orography-induced turbulence in a mesobeta-scale model. *Mon. Wea. Rev.*, **117**, 1872–1890, [https://doi.org/10.1175/1520-0493\(1989\)117<1872:POOITI>2.0.CO;2](https://doi.org/10.1175/1520-0493(1989)117<1872:POOITI>2.0.CO;2).
- Chen, F., X. Yang, and W. Zhu, 2014: WRF simulations of urban heat island under hot-weather synoptic conditions: The case study of Hangzhou City, China. *Atmos. Res.*, **138**, 364–377, <https://doi.org/10.1016/j.atmosres.2013.12.005>.
- Chou, M.-D., and M. J. Suarez, 1999: A solar radiation parameterization for atmospheric studies. NASA Technical Report Series on Global Modeling and Data Assimilation, M. J. Suarez, Ed., NASA Tech. Memo. NASA/TM-1999-104606, Vol. 15, 51 pp., <https://gmao.gsfc.nasa.gov/pubs/docs/Chou136.pdf>.
- Cook, N. J., 1997: The Deaves and Harris ABL model applied to heterogeneous terrain. *J. Wind Eng. Ind. Aerodyn.*, **66**, 197–214, [https://doi.org/10.1016/S0167-6105\(97\)00034-2](https://doi.org/10.1016/S0167-6105(97)00034-2).
- Dissanayake, D., T. Morimoto, Y. Murayama, M. Ranagalage, and H. H. Handayani, 2019: Impact of urban surface characteristics and socio-economic variables on the spatial variation of land surface temperature in Lagos City, Nigeria. *Sustainability*, **11**, 25, <https://doi.org/10.3390/su11010025>.
- Doan, Q.-V., and H. Kusaka, 2016: Numerical study on regional climate change due to the rapid urbanization of greater Ho Chi Minh City's metropolitan area over the past 20 years. *Int. J. Climatol.*, **36**, 3633–3650, <https://doi.org/10.1002/joc.4582>.

- Doan, V. Q., and H. Kusaka, 2018: Projections of urban climate in the 2050s in a fast-growing city in Southeast Asia: The greater Ho Chi Minh City metropolitan area, Vietnam. *Int. J. Climatol.*, **38**, 4155–4171, <https://doi.org/10.1002/joc.5559>.
- Droste, A. M., G. J. Steeneveld, and A. A. M. Holtslag, 2018: Introducing the urban wind island effect. *Environ. Res. Lett.*, **13**, 094007, <https://doi.org/10.1088/1748-9326/aad8ef>.
- Dudhia, J., 1989: Numerical study of convection observed during the winter monsoon experiment using a mesoscale two-dimensional model. *J. Atmos. Sci.*, **46**, 3077–3107, [https://doi.org/10.1175/1520-0469\(1989\)046<3077:NSOCOD>2.0.CO;2](https://doi.org/10.1175/1520-0469(1989)046<3077:NSOCOD>2.0.CO;2).
- Grimm, N. B., S. H. Faeth, N. E. Golubiewski, C. L. Redman, J. Wu, X. Bai, and J. M. Briggs, 2008: Global change and the ecology of cities. *Science*, **319**, 756–760, <https://doi.org/10.1126/science.1150195>.
- Grossman-Clarke, S., J. A. Zehnder, T. Loridan, and C. S. B. Grimmond, 2010: Contribution of land use changes to near-surface air temperatures during recent summer extreme heat events in the Phoenix metropolitan area. *J. Appl. Meteor. Climatol.*, **49**, 1649–1664, <https://doi.org/10.1175/2010JAMC2362.1>.
- Haeger-Eugensson, M., and B. Holmer, 1999: Advection caused by the urban heat island circulation as a regulating factor on the nocturnal urban heat island. *Int. J. Climatol.*, **19**, 975–988, [https://doi.org/10.1002/\(SICI\)1097-0088\(199907\)19:9<975::AID-JOC399>3.0.CO;2-J](https://doi.org/10.1002/(SICI)1097-0088(199907)19:9<975::AID-JOC399>3.0.CO;2-J).
- Han, L., W. Zhou, and W. Li, 2016: Fine particulate ( $\text{PM}_{2.5}$ ) dynamics during rapid urbanization in Beijing, 1973–2013. *Sci. Rep.*, **6**, 23604, <https://doi.org/10.1038/srep23604>.
- Heaviside, C., S. Vardoulakis, and X. M. Cai, 2016: Attribution of mortality to the urban heat island during heatwaves in the West Midlands, UK. *Environ. Health*, **15**, S27, <https://doi.org/10.1186/s12940-016-0100-9>.
- , H. Macintyre, and S. Vardoulakis, 2017: The urban heat island: Implications for health in a changing environment. *Curr. Environ. Health Rep.*, **4**, 296–305, <https://doi.org/10.1007/s40572-017-0150-3>.
- Hong, S.-Y., J. Dudhia, and S.-H. Chen, 2004: A revised approach to ice microphysical processes for the bulk parameterization of clouds and precipitation. *Mon. Wea. Rev.*, **132**, 103–120, [https://doi.org/10.1175/1520-0493\(2004\)132<0103:ARATIM>2.0.CO;2](https://doi.org/10.1175/1520-0493(2004)132<0103:ARATIM>2.0.CO;2).
- Hoornweg, D., and K. Pope, 2017: Population predictions for the world's largest cities in the 21st century. *Environ. Urban.*, **29**, 195–216, <https://doi.org/10.1177/0956247816663557>.
- Hussaini, A., and S. O. Yakubu, 2019: Automation and modernization of meteorological observation network in Nigeria. *J. Appl. Sci. Environ. Manage.*, **23**, 1225, <https://doi.org/10.4314/jasem.v23i7.6>.
- Iacono, M. J., J. S. Delamere, E. J. Mlawer, M. W. Shephard, S. A. Clough, and W. D. Collins, 2008: Radiative forcing by long-lived greenhouse gases: Calculations with the AER radiative transfer models. *J. Geophys. Res.*, **113**, D13103, <https://doi.org/10.1029/2008JD009944>.
- IPCC, 2013: *Climate Change 2013: The Physical Science Basis*. Cambridge University Press, 1535 pp., <https://doi.org/10.1017/CBO9781107415324>.
- Jackson, T. L., J. J. Feddema, K. W. Oleson, G. B. Bonan, and J. T. Bauer, 2010: Parameterization of urban characteristics for global climate modeling. *Ann. Assoc. Amer. Geogr.*, **100**, 848–865, <https://doi.org/10.1080/00045608.2010.497328>.
- Janjić, Z. I., 1994: The step-mountain eta coordinate model: Further developments of the convection, viscous sublayer, and turbulence closure schemes. *Mon. Wea. Rev.*, **122**, 927–945, [https://doi.org/10.1175/1520-0493\(1994\)122<0927:TSMECM>2.0.CO;2](https://doi.org/10.1175/1520-0493(1994)122<0927:TSMECM>2.0.CO;2).
- Jerez, S., J. P. Montavez, P. Jimenez-Guerrero, J. J. Gomez-Navarro, R. Lorente-Plazas, and E. Zorita, 2013: A multi-physics ensemble of present-day climate regional simulations over the Iberian Peninsula. *Climate Dyn.*, **40**, 3023–3046, <https://doi.org/10.1007/s00382-012-1539-1>.
- Jiboye, A. D., and L. O. Ogunshakin, 2011: Urban growth challenges in Nigeria: Implications for environmental sustainability. *Br. J. Humanit. Soc. Sci.*, **1**, 16–27.
- Kalnay, E., and M. Cai, 2003: Impact of urbanization and land-use change on climate. *Nature*, **423**, 528–531, <https://doi.org/10.1038/nature01675>.
- Kim, Y., K. Sartelet, J.-C. Raut, and P. Chazette, 2013: Evaluation of the Weather Research and Forecast/urban model over greater Paris. *Bound.-Layer Meteor.*, **149**, 105–132, <https://doi.org/10.1007/s10546-013-9838-6>.
- Kusaka, H., H. Kondo, Y. Kikegawa, and F. Kimura, 2001: A simple single-layer urban canopy model for atmospheric models: Comparison with multi-layer and slab models. *Bound.-Layer Meteor.*, **101**, 329–358, <https://doi.org/10.1023/A:1019207923078>.
- , F. Chen, M. Tewari, J. Dudhia, D. O. Gill, M. G. Duda, W. Wang, and Y. Miya, 2012: Numerical simulation of urban heat island effect by the WRF model with 4-km grid increment: An inter-comparison study between the urban canopy model and slab model. *J. Meteor. Soc. Japan*, **90B**, 33–45, <https://doi.org/10.2151/jmsj.2012-B03>.
- Laux, P., P. N. B. Nguyen, J. Cullmann, T. P. Van, and H. Kunstmann, 2017: How many RCM ensemble members provide confidence in the impact of land-use/land cover change? *Int. J. Climatol.*, **37**, 2080–2100, <https://doi.org/10.1002/joc.4836>.
- Li, D., and E. Bou-Zeid, 2013: Synergistic interactions between urban heat islands and heat waves: The impact in cities is larger than the sum of its parts. *J. Appl. Meteor. Climatol.*, **52**, 2051–2064, <https://doi.org/10.1175/JAMC-D-13-02.1>.
- Li, X. X., T. Y. Koh, D. Entekhabi, M. Roth, J. Panda, and L. K. Norford, 2013: A multi-resolution ensemble study of a tropical urban environment and its interactions with the background regional atmosphere. *J. Geophys. Res. Atmos.*, **118**, 9804–9818, <https://doi.org/10.1002/jgrd.50795>.
- Loridan, T., F. Lindberg, O. Jorba, S. Kotthaus, S. Grossman-Clarke, and C. S. B. Grimmond, 2013: High resolution simulation of the variability of surface energy balance fluxes across central London with urban zones for energy partitioning. *Bound.-Layer Meteor.*, **147**, 493–523, <https://doi.org/10.1007/s10546-013-9797-y>.
- Lucas-Picher, P., D. Caya, S. Biner, and R. Laprise, 2008: Quantification of the lateral boundary forcing of a regional climate model using an aging tracer. *Mon. Wea. Rev.*, **136**, 4980–4996, <https://doi.org/10.1175/2008MWR2448.1>.
- McCarthy, M. P., M. J. Best, and R. A. Betts, 2010: Climate change in cities due to global warming and urban effects. *Geophys. Res. Lett.*, **37**, L09705, <https://doi.org/10.1029/2010GL042845>.
- McGrane, S. J., 2016: Impacts of urbanisation on hydrological and water quality dynamics, and urban water management: A review. *Hydrol. Sci. J.*, **61**, 2295–2311, <https://doi.org/10.1080/02626667.2015.1128084>.
- Miao, S., F. Chen, M. A. LeMone, M. Tewari, Q. Li, and Y. Wang, 2009: An observational and modeling study of characteristics of urban heat island and boundary layer structures in Beijing. *J. Appl. Meteor. Climatol.*, **48**, 484–501, <https://doi.org/10.1175/2008JAMC1909.1>.

- Moghadam, S. H., and M. Helbich, 2013: Spatiotemporal urbanization processes in the megacity of Mumbai, India: A Markov chains-cellular automata urban growth model. *Appl. Geogr.*, **40**, 140–149, <https://doi.org/10.1016/j.apgeog.2013.01.009>.
- Mohan, M., S. K. Pathan, K. Narendrareddy, A. Kandy, and S. Pandey, 2011: Dynamics of urbanization and its impact on land-use/land-cover: A case study of megacity Delhi. *J. Environ. Prot.*, **02**, 1274–1283, <https://doi.org/10.4236/jep.2011.29147>.
- Mora, C., and Coauthors, 2017: Global risk of deadly heat. *Nat. Climate Change*, **7**, 501–506, <https://doi.org/10.1038/nclimate3322>.
- Morris, C. J. G., I. Simmonds, and N. Plummer, 2001: Quantification of the influences of wind and cloud on the nocturnal urban heat island of a large city. *J. Appl. Meteor.*, **40**, 169–182, [https://doi.org/10.1175/1520-0450\(2001\)040<0169:QOTIOW>2.0.CO;2](https://doi.org/10.1175/1520-0450(2001)040<0169:QOTIOW>2.0.CO;2).
- Morris, K. I., A. Chan, K. J. K. Morris, M. C. G. Ooi, M. Y. Oozeer, Y. A. Abakr, M. S. M. Nadzir, and I. Y. Mohammed, 2017: Urbanisation and urban climate of a tropical conurbation, Klang Valley, Malaysia. *Urban Climate*, **19**, 54–71, <https://doi.org/10.1016/j.uclim.2016.12.002>.
- NOAA/NCEI, 2019: Climate at a Glance: Global time series. Accessed 28 October 2019, <https://www.ncdc.noaa.gov/cag/global/time-series>.
- NOAA/NCEP, 2000: NCEP FNL Operational Model Global Tropospheric Analyses, continuing from July 1999 (updated daily). National Center for Atmospheric Research Computational and Information Systems Laboratory Research Data Archive, accessed 4 January 2018, <https://doi.org/10.5065/D6M043C6>.
- Obiefuna, J., P. C. Nwilo, A. O. Atagbaza, and C. J. Okolie, 2013: Spatial changes in the wetlands of Lagos/Lekki Lagoons of Lagos, Nigeria. *J. Sustain. Dev.*, **6**, 123–133, <https://doi.org/10.5539/jsd.v6n7p123>.
- Ojeh, V., A. Balogun, and A. Okhimamhe, 2016: Urban-rural temperature differences in Lagos. *Climate*, **4**, 29, <https://doi.org/10.3390/cli4020029>.
- Oke, T. R., 1973: City size and the urban heat island. *Atmos. Environ.*, **7**, 769–779, [https://doi.org/10.1016/0004-6981\(73\)90140-6](https://doi.org/10.1016/0004-6981(73)90140-6).
- , 1982: The energetic basis of the urban heat island. *Quart. J. Roy. Meteor. Soc.*, **108**, 1–24, <https://doi.org/10.1002/qj.49710845502>.
- Opoko, A. P., and A. Oluwatayo, 2014: Trends in urbanisation: Implication for planning and low-income housing delivery in Lagos, Nigeria. *Archit. Res.*, **4**, 15–26, <https://doi.org/10.5923/s.arch.201401.03>.
- Ouyang, T., Z. Zhu, and Y. Kuang, 2006: Assessing impact of urbanization on river water quality in the Pearl River Delta economic zone, China. *Environ. Monit. Assess.*, **120**, 313–325, <https://doi.org/10.1007/s10661-005-9064-x>.
- Pal, S., and Coauthors, 2012: Spatio-temporal variability of the atmospheric boundary layer depth over the Paris agglomeration: An assessment of the impact of the urban heat island intensity. *Atmos. Environ.*, **63**, 261–275, <https://doi.org/10.1016/j.atmosenv.2012.09.046>.
- Pesaresi, M., and Coauthors, 2016: Operating procedure for the production of the Global Human Settlement Layer from Landsat data of the epochs 1975, 1990, 2000, and 2014. European Union Publications Office Rep., 62 pp., [http://publications.jrc.ec.europa.eu/repository/bitstream/JRC97705/landsatgs\\_report\\_2016\\_final\\_online.pdf](http://publications.jrc.ec.europa.eu/repository/bitstream/JRC97705/landsatgs_report_2016_final_online.pdf).
- Roth, M., 2007: Review of urban climate research in (sub)tropical regions. *Int. J. Climatol.*, **27**, 1859–1873, <https://doi.org/10.1002/joc.1591>.
- Sailor, D. J., M. Georgescu, J. M. Milne, and M. A. Hart, 2015: Development of a national anthropogenic heating database with an extrapolation for international cities. *Atmos. Environ.*, **118**, 7–18, <https://doi.org/10.1016/j.atmosenv.2015.07.016>.
- Santamouris, M., 2015: Analyzing the heat island magnitude and characteristics in one hundred Asian and Australian cities and regions. *Sci. Total Environ.*, **512–513**, 582–598, <https://doi.org/10.1016/j.scitotenv.2015.01.060>.
- Seto, K. C., B. Guneralp, and L. R. Hutyra, 2012: Global forecasts of urban expansion to 2030 and direct impacts on biodiversity and carbon pools. *Proc. Natl. Acad. Sci. USA*, **109**, 16 083–16 088, <https://doi.org/10.1073/pnas.1211658109>.
- Simm, W. A., F. Samreen, R. Bassett, M. A. Ferrario, G. Blair, J. Whittle, and P. J. Young, 2018: SE in ES: Opportunities for software engineering and cloud computing in environmental science. *Proc. 40th Int. Conf. on Software Engineering: Software Engineering in Society—ICSE-SEIS '18*, New York, NY, ACM Press, 61–70, <https://doi.org/10.1145/3183428.3183430>.
- Simwanda, M., M. Ranagalage, R. C. Estoque, and Y. Murayama, 2019: Spatial analysis of surface urban heat islands in four rapidly growing African cities. *Remote Sens.*, **11**, 1645, <https://doi.org/10.3390/rs11141645>.
- Skamarock, W. C., and Coauthors, 2008: A description of the Advanced Research WRF version 3. NCAR Tech. Note NCAR/TN-475+STR, 113 pp., <https://doi.org/10.5065/D68S4MVH>.
- Theeuwes, N. E., G.-J. Steeneveld, R. J. Ronda, M. W. Rotach, and A. A. M. Holtslag, 2015: Cool city mornings by urban heat. *Environ. Res. Lett.*, **10**, 114022, <https://doi.org/10.1088/1748-9326/10/11/114022>.
- Thompson, G., P. R. Field, R. M. Rasmussen, and W. D. Hall, 2008: Explicit forecasts of winter precipitation using an improved bulk microphysics scheme. Part II: Implementation of a new snow parameterization. *Mon. Wea. Rev.*, **136**, 5095–5115, <https://doi.org/10.1175/2008MWR2387.1>.
- United Nations, 2015: World Urbanization Prospects: The 2014 revision. United Nations Department of Economic and Social Affairs Rep., 517 pp., <https://population.un.org/wup/Publications/Files/WUP2014-Report.pdf>.
- Wang, X., and Y. Li, 2016: Predicting urban heat island circulation using CFD. *Build. Environ.*, **99**, 82–97, <https://doi.org/10.1016/j.buildenv.2016.01.020>.
- Wilby, R. L., 2008: Constructing climate change scenarios of urban heat island intensity and air quality. *Environ. Plann.*, **35B**, 902–919, <https://doi.org/10.1068/b33066t>.
- Yin, J., Z. Yin, H. Zhong, S. Xu, X. Hu, J. Wang, and J. Wu, 2011: Monitoring urban expansion and land use/land cover changes of Shanghai metropolitan area during the transitional economy (1979–2009) in China. *Environ. Monit. Assess.*, **177**, 609–621, <https://doi.org/10.1007/s10661-010-1660-8>.
- Zhang, N., X. Wang, and Z. Peng, 2014: Large-eddy simulation of mesoscale circulations forced by inhomogeneous urban heat island. *Bound.-Layer Meteor.*, **151**, 179–194, <https://doi.org/10.1007/s10546-013-9879-x>.
- Zhao, L., X. Lee, R. B. Smith, and K. Oleson, 2014: Strong contributions of local background climate to urban heat islands. *Nature*, **511**, 216–219, <https://doi.org/10.1038/nature13462>.